Trabajo Fin de Máster

Production of High-Energy Solar Neutrinos in a Dark Matter Model

Pablo de la Torre Domínguez

Julio de 2023

UNIVERSIDAD DE GRANADA

Tutor: Manuel Masip Mellado

Depto. Física Teórica y del Cosmos, UGR

Firma Tutor:

MASIP MELLADO MANUEL - 35043277V

Digitally signed by MASIP MELLADO MANUEL - 35043277V
Date: 2023.07.07 12:49:26 +02'00'

Resumen

En este trabajo hemos estudiado un modelo de partícula exótica que podría explicar la materia oscura del universo. Primero hemos introducido brevemente nuestro modelo de universo, conocido como ΛCDM, y hemos revisado las condiciones que debe reunir un candidato viable a ser la materia oscura. Luego hemos definido nuestro modelo, donde los ingredientes básicos son una WIMP fermiónica χ con una masa entre 50 y 1000 GeV que se acopla con la materia ordinaria sólo a través del bosón de Higgs y un neutrino estéril de Dirac N con una masa similar. El neutrino estéril introduce acoplos de Yukawa con el Higgs de tipo $hN\nu$, lo que implicaría la producción de de neutrinos monocromáticos en la aniquilación de la materia oscura, $\chi\bar{\chi} \to N\nu$. Por último, calculamos el flujo de neutrinos de alta energía que podría producir este tipo de materia oscura tras ser atrapada por el Sol. Los flujos solares de alta energía son buscados en telescopios de neutrinos como KM3NeT. Finalmente, mencionar que, dados los buenos resultados obtenidos, estamos preparando un artículo, que esperamos tener listo en unas semanas.

Palabras Clave: Materia oscura, Higgs portal, neutrinos

Abstract

In this paper we have studied an exotic particle model that could explain the dark matter (DM) in the Universe. First of all, we have introduced our Universe model, known as ΛCDM, and we have reviewed the conditions that a DM candidate must have. Later, we have defined our own model, where the basic ingredients are a fermionic WIMP χ with a mass between 50 and 1000 GeV that couples to ordinary matter only through Higgs boson, and a sterile Dirac neutrino N with a similar mass. The sterile neutrino introduces Yukawa couplings with the Higgs boson such as $hN\nu$, which would imply the production of monochromatic neutrinos in DM annihilation $\chi\bar{\chi} \to N\nu$. Eventually, we calculate the high energy neutrino flux that could be produced DM after being trapped at the Sun. The solar high energy neutrino fluxes are searched in neutrino telescopes such as KM3NeT. Finally, to mention that following the good results obtained, we are preparing a paper that we hope to have ready in a few weeks.

Key words: Dark matter, Higgs portal, neutrinos

Contents

1 Introduction: The Dark Matter Mystery

There are several observations suggesting that there is matter in the Universe that, in contrast to stars and to interstellar gas, does not emit light, it is *dark*. Some of the evidences for the dark matter existence are:

- Rotation Curves of Galaxies: Newton dynamics indicate the presence of extra mass in the galaxy.

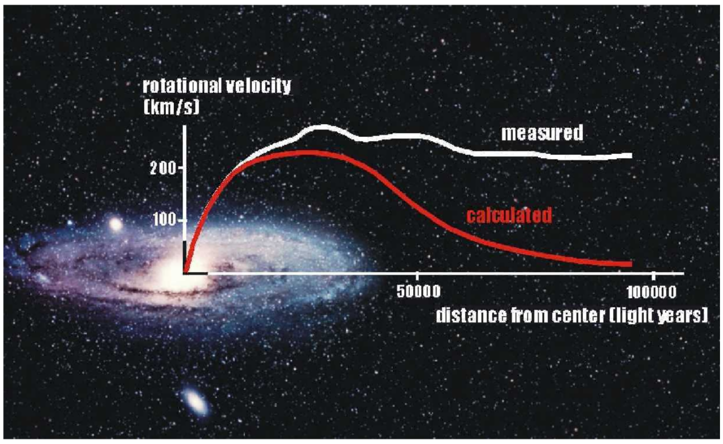

Figure 1: Calculated and observed rotation curve of the Andromeda galaxy [1].

- Gravitational Lensing: Following General Relativity, the gravitational lensing that we observe can only be produced if there is extra non-luminous matter.

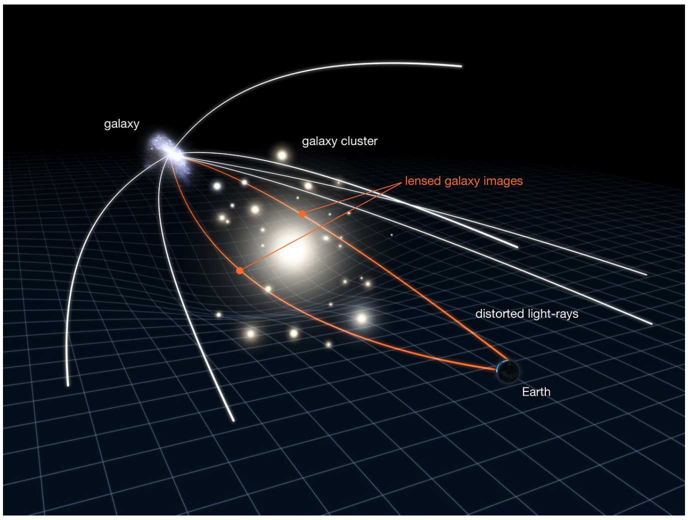

Figure 2: Scheme of a gravitational lense [2].

- Structure Formation: If there were only ordinary matter in the Universe, there would not have been enough time for density perturbations to grow and form galaxies and clusters.

- CMB anisotropies: the ratio between the first and second peaks (see Figure 3) in the angular correlation of temperature fluctuations indicates that there are 5 grams of dark matter per each gram of baryonic matter.

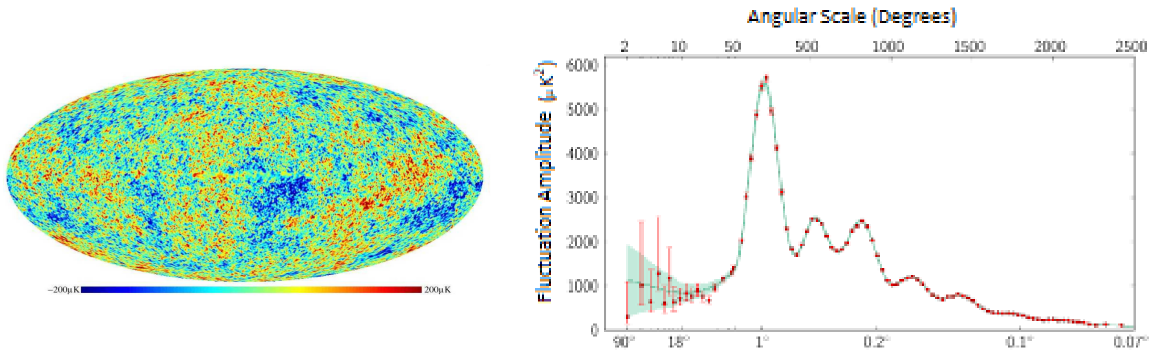

Figure 3: Cosmic Microwave Background [3].

Despite all these "gravitational" evidences, no experiment has still detected dark matter (DM): we do not know the mass nor the fermionic or bosonic nature of the particle that constitutes it, and we do not know if it interacts with the visible matter only through gravity or there are other mediators.

In this work we will focus on a candidate, the weakly interacting massive particle (WIMP) that has been studied for many years. A WIMP could be seen in a *direct* search experiment when it crosses a detector and hits a nucleus or in an *indirect* search experiment, where we would see the high energy particles produced when a pair of DM particles annihilate in the center of the galaxy or the Sun. Here we will be interested on the indirect neutrino signal that a WIMP trapped in the Sun may produce. In particular, our objective is to define a particle physics model that gives an optimal signal at neutrino telescopes.

2 Cosmological model

Let us start by briefly reviewing the main features of our model of Universe, that is formulated in the framework of the General Relativity. It is based on the cosmological principle: on scales large enough (larger than a galaxy) the Universe is homogeneous and isotropic. Its kinematics will be described by a metric, and the only one consistent with this principle is the so-called Friedmann–Lemaître–Robertson–Walker (FLRW) metric

$$\mathrm{d}s^2 = dt^2 - a^2(t)\left(\frac{dr^2}{1-kr^2} + r^2 d\theta^2 + r^2 sin^2\theta d\phi^2\right). \tag{2.1}$$

We will refer (t, r, θ, ϕ) as the comoving coordinates, r is a dimensionless coordinate that takes values between 0 and 1, whereas $a(t)$ is the cosmic scale factor (with dimensions of space) and k is the curvature parameter, which after a rescaling can be chosen $+1$, -1 or 0 for positive, negative, or zero spatial curvature, respectively.

The physical meaning of these two parameters can be easily understood with an example. Let us parameterize a circumference in this space and obtain its length ℓ and radius R. We place the center at the point with comoving coordinates $t=0$, $r=0$ and the circumference in the XY plane.

The points in the circumference can be parameterized as $(t=0, r=r_0, \theta=\pi/2, \phi\in[0,2\pi))$, whereas the points in a radius at a fixed value of ϕ are $(t=0, r\in[0,r_0], \theta=\pi/2, \phi=\phi_0)$. The length ℓ of the circumference is then

$$\ell = \int_0^{2\pi} -\sqrt{g_{\phi\phi}}\,\mathrm{d}\phi = \int_0^{2\pi} a(t)\,r_0\,d\phi = 2\pi\,a(t)\,r_0. \tag{2.2}$$

To obtain the radius we integrate

$$R = \int_0^{r_0} -\sqrt{g_{rr}}\,\mathrm{d}r = \int_0^{r_0} \frac{a(t)}{\sqrt{1-kr^2}}\,\mathrm{d}r, \tag{2.3}$$

in terms of the three possible values of k, it will be:

$$\begin{cases} R = a(t)\,\mathrm{ArcSin}(r_0) & (k=+1) \\ R = a(t)\,r_0 & (k=0) \\ R = a(t)\,\mathrm{ArcSinh}(r_0) & (k=-1). \end{cases} \tag{2.4}$$

We see that

i) The ratio ℓ/R is smaller than 2π for $k=+1$ (just like in the surface of a sphere or any surface with positive curvature), 2π for $k=0$ (like in a space with euclidean geometry or any surface without curvature) and larger than 2π for $k=+1$ (like in surfaces with negative curvature).

ii) Distances are proportional to the scale factor: if $a(t)$ doubles from t_1 to t_2, the length of the circumference doubles (so those same points at t_1 will be twice as far at t_2) as well in that difference of time, even though its comoving coordinates are constant. The circumference would grow like if it were drawn in a balloon that is swelling up. This can be interpreted as an expansion of the Universe, which is illustrated in Figure 4.

Experimentally, we find that our Universe has zero curvature [4], which could be explained if it went through a period of exponential inflation: any sphere that is *inflated* looks flat, with zero curvature. We will then assume $k=0$. In addition to the homogeneity and isotropy of our

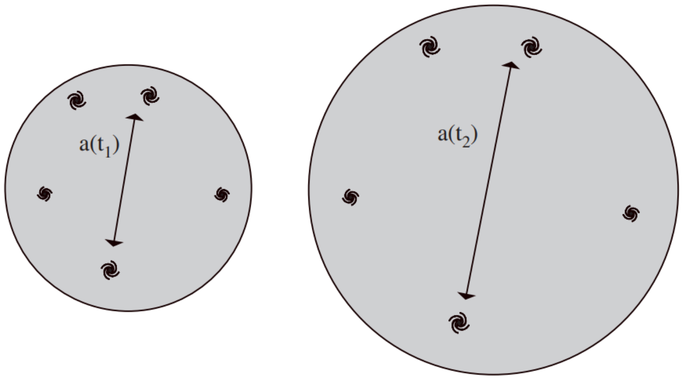

Figure 4: Scheme of an expanding Universe. The size and pattern of location of individual galaxies are the same, but all distances have been stretched by the scale factor.

Universe, a second basic observation is that it is not static, it is an expanding Universe. This will be described with the evolution of $a(t)$: as the scale factor grows, the Universe expands. Moreover, in the 1920's it was observed that the light of all galaxies is redshifted: they are moving away from us, and the further they are, the faster they are moving, being the constant of proportionality the so-called Hubble constant H_0. The metric of FLRW is also consistent with this redshift: since any physical length measured in t must be proportional to $a(t)$, the wavelength of a photon at two different times t_1 and t_2 will satisfy

$$\frac{\lambda_1}{\lambda_2} = \frac{a(t_1)}{a(t_2)}. \tag{2.5}$$

This result can also be obtained by considering the propagation of light on a geodesic ($ds^2 = 0$). In an analogous way, a particle will lose velocity as the Universe expands.

Astronomers define the redshift z of an object in terms of the ratio of the detected wavelength to the emitted wavelength at an earlier time,

$$1 + z \equiv \frac{\lambda_2}{\lambda_1} = \frac{a(t_2)}{a(t_1)}. \tag{2.6}$$

If we expand the scale factor around the present epoch t_0

$$\begin{aligned} \frac{a(t)}{a(t_0)} =& 1 + \frac{\dot{a}(t_0)}{a(t_0)}(t - t_0) + \frac{1}{2}\ddot{a}(t)(t - t_0)^2 + \ldots \\ =& 1 + H_0 (t - t_0) - \frac{1}{2} q_0 H_0^2 (t - t_0)^2 + \ldots, \end{aligned} \tag{2.7}$$

it is easy to relate the Hubble constant with the redshift through the so-called Hubble's law:

$$H_0 d_L = z + \frac{1}{2}(1 - q_0) z^2 + \cdots \approx z, \tag{2.8}$$

where d_L is the distance deduced from the luminosity of a galaxy.

3 Evolution of the Universe

Dynamics

The dynamics of the universe, i.e., how the scale factor changes with time, is dictated by Einstein's equations

$$G_{\mu\nu} \equiv R_{\mu\nu} - \frac{1}{2} g_{\mu\nu} R = 8\pi G T_{\mu\nu}. \tag{3.1}$$

The FLRW metric is diagonal, so the stress-energy tensor $T_{\mu\nu}$ that produces it will also be diagonal. In addition, isotropy implies that the spatial components coincide; the simplest realization of a stress-energy tensor fulfilling these conditions corresponds to a perfect fluid, characterized by a time-dependent energy density $\rho(t)$ and pressure $p(t)$

$$T^{\mu}_{\nu} = diag(\rho, -p, -p, -p, -p). \tag{3.2}$$

Imposing the conservation of the stress energy tensor ($\nabla_\mu T^{\mu\nu} = 0$) and assuming a perfect fluid with state equation

$$p = \omega\rho\,, \tag{3.3}$$

we obtain how the energy density depends on the scale factor:

$$\rho \propto a^{-3(1+\omega)}\,. \tag{3.4}$$

In particular, for different kinds of perfect fluids we find

$$\begin{cases} \text{Radiation}: & \omega = 1/3, \quad \rho \propto a^{-4} \\ \text{Matter}: & \omega = 0, \quad\;\;\; \rho \propto a^{-3} \\ \text{Vacuum } Energy: & \omega = -1, \quad \rho \propto const. \end{cases} \tag{3.5}$$

We can understand the three types of fluid at the microscopic level. A comoving volume grows like a^3, and the number of particles inside that volume is constant. In a fluid of matter (particles with a negligible kinetic energy and an energy close to the rest mass), the energy density dilutes just because the comoving volume grows, it goes like $1/a^3$. In contrast, in a fluid of radiation (particles with a negligible rest mass) their energy redshifts with the expansion, implying an extra factor of a, so ρ goes like $1/a^4$. In a fluid of vacuum the energy density does not change with the expansion.

To know how the Universe evolves, we must obtain the Ricci Tensor and Ricci Scalar for the FLRW metric and substitute it in the Einstein Equations. For the 0-0 we obtain the so-called Friedmann equation:

$$1 + \frac{k}{H^2 a^2} = \frac{\rho}{3H^2 m_p^2} \equiv \frac{\rho}{\rho_c}\,. \tag{3.6}$$

In this equation m_p is the Planck mass and we have obtained the critical density $\rho_c = 3H^2 m_p^2$. Notice that, if $\rho = \rho_c$, then $k = 0$: ρ_c is the energy density for the Universe to be flat. As we have mentioned before, the data suggests that the energy density of matter, radiation and vacuum adds to ρ_c. It is useful to express how each component of the fluid contributes to the critical energy density as it abundance, $\Omega_\alpha = \rho_\alpha / \rho_c$.

Experimentally, CMB observables tell us that [4][1]:

$$\Omega_{DM} h^2 = 0.120 \pm 0.001\,, \tag{3.7}$$

where h is the reduced Hubble constant related to H_0 by

$$H_0 = 100\,h\;Km\;s^{-1} Mpc^{-1}. \tag{3.8}$$

Thermal equilibrium

The early Universe was to a good approximation in thermodynamic equilibrium. This means that the reactions that change the number and energy distribution of particles that dictate the expansion, occurred much faster than the expansion rate of the Universe. Then, for each moment they are described by a Fermi-Dirac (fermions) or a Bose-Einstein (boson) distribution,

$$\begin{cases} f_f = \dfrac{1}{e^{(E-\mu)/T} + 1}\,, \\ f_b = \dfrac{1}{e^{(E-\mu)/T} - 1}\,. \end{cases} \tag{3.9}$$

In addition, it is also a good approximation to assume the conservation of the total entropy in a comoving volume, *i.e.*, there is no transfer of heat from one comoving region to another in the early Universe. In contrast, the energy contained in a comoving volume does change: for a fluid of radiation, the non-zero pressure implies that it does work and loses energy when it volume expands and loses energy ($\mathrm{d}W = -p\mathrm{d}V$). This accounts for the redshift and the extra a factor in the radiation case. The entropy in a comoving volume is then a very useful fiducial quantity during the expansion of the Universe as it remains constant, as long as thermal equilibrium is maintained.

Abundance of a massive species and freeze out

Consider a heavy particle Φ of mass m_Φ that can react to give light particles ϕ, $\Phi\bar{\Phi} \leftrightarrow \phi\bar{\phi}$. A comoving volume grows like a^3. On the other hand, as the total entropy does not change, the entropy density must dilutes like $s \propto a^{-3}$ due to the expansion. As a consequence, the ratio

[1]The dark matter density is sometimes expressed in the bibliography as $\Omega_c h^2$, referring to Cold dark matter. Instead, we will use $\Omega_{DM} h^2$ for greater clarity.

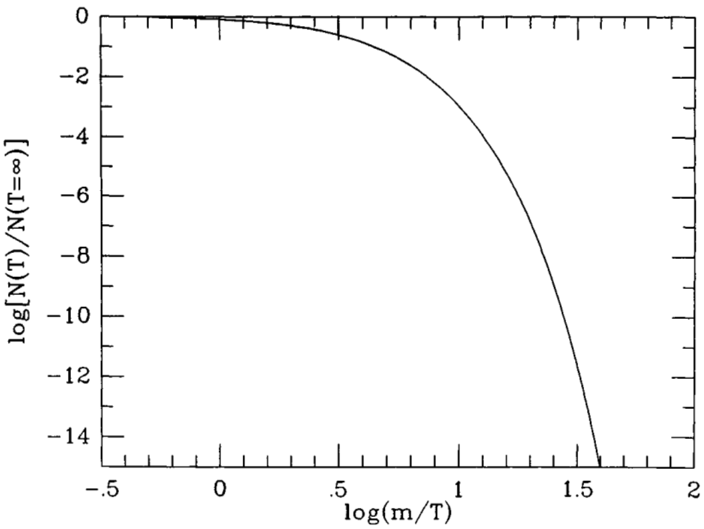

Figure 5: The equilibrium abundance of a species in a comoving volume element, $N_{EQ} = Y_{EQ} = n_{EQ}/s$, in terms of $x = m/T$. Here it is represented the logarithm of each quantity, and N_{EQ} is normalized to its abundance in the early Universe $N(T = \infty)$ [7].

of the number density of particles Φ to s, n_Φ/s, will be proportional to the total number of particles of type Φ in a comoving volume. We define this ratio as the abundance Y_Φ of the species Φ. The abundance of a species in equilibrium is [5]

$$Y_{\Phi,EQ} \equiv \frac{n_{\Phi,EQ}}{s} = \frac{45}{4\pi^4}\frac{g_\Phi}{g_{*s}} x^2 K_2(x)\,, \tag{3.10}$$

where $x = m_\Phi/T$, g_Φ counts the degrees of freedom in the species Φ (*e.g.*, 4 for an electron or 2 for a neutrino), and g_{*S} is a variable that depends on the total number of effectively massless degrees of freedom in the thermal bath. Its value at temperatures above the top quark mass is 106.75 (see more in [6, 7]). Using g_{*S} the entropy density can be expressed as

$$s = \frac{2\pi^2}{45} g_{*s} T^3\,. \tag{3.11}$$

The equilibrium abundance when Φ is relativistic (at temperatures larger than the mass m_Φ) can be expressed as

$$Y_{\Phi,EQ} = \frac{45\zeta(3)g}{2\pi^4 g_{*s}} \qquad (T >> m_\Phi)\,, \tag{3.12}$$

whereas, at temperatures below m_Φ, equilibrium thermodynamics dictates that the reaction $\Phi\bar{\Phi} \leftrightarrow \phi\bar{\phi}$ is tilted to the right and the number density of Φ decreases exponentially:

$$Y_{\Phi,EQ} = \frac{45g}{4\sqrt{2}\pi^5 g_{*s}} \left(\frac{m_\Phi}{T}\right)^{3/2} e^{-m_\Phi/T} \qquad (T << m_\Phi)\,. \tag{3.13}$$

In Figure 5, we represent the equilibrium abundance as a function of x.

But as Universe expands and the density of particles type H decreases, it becomes more rare for them to collide and annihilate. But, the equilibrium will only hold as long as there are interactions with other particles, which link Φ to the thermal bath,

$$\text{Equilibrium} \iff \text{Interactions.} \tag{3.14}$$

So, when the reactions stop, the species Φ decouples, it goes "out of thermal equilibrium" and its abundance *freezes out* (becomes constant). To estimate at what temperature the freeze out occurs, we may just compare the interaction rate $\Gamma_I \equiv n_\Phi \langle \sigma |v| \rangle$ with the expansion rate of the Universe H: if the probability for a reaction is small during the time the Universe doubles it size ($\approx 1/H$), the probability that it occurs afterwards is negligible. In order to know if the particle Φ is coupled or not, we can use this rule

$$\begin{aligned} &\Gamma_I \gtrsim H \quad \text{(coupled)} \\ &\Gamma_I \lesssim H \quad \text{(decoupled)}. \end{aligned} \tag{3.15}$$

When the particle species Φ decouples, its number density will decrease only due to the increase in the volume, as Universe expands. Since volume increases as a^3 and the number of particles remain constant, the number density will decrease as a^{-3}. In addition, if the particle species Φ is very massive, it will decouple when it is no longer relativistic (when $m_\Phi \lesssim T$, so it behaves like matter), so, once decoupled, its energy density will decrease as a^{-3}. At this point ρ_Φ will represent a small contribution to the total energy density of the Universe, dominated by radiation. However, since ρ_{rad} evolves like a^{-4} with the expansion, as a grows there will be a point that ρ_Φ will dominate: this is exactly what we need to explain the dark matter of the Universe with a WIMP.

Let us be more specific. Consider a Dirac particle χ and its antiparticle $\bar{\chi}$ with zero chemical potential (same abundance at all temperatures). Using Boltzmann equation is easy to obtain its abundance at a given value of temperature T ($x = m_\chi/T$),

$$\frac{\mathrm{d}Y_\chi}{\mathrm{d}x} = \frac{-x\,\langle \sigma_{\mathrm{ann}}|v|\rangle s}{H(m)}\left(Y^2 - Y_{EQ}^2\right) \tag{3.16}$$

where Y_{EQ} is the equilibrium abundance defined in Equation (3.10) and $\langle \sigma_{\mathrm{ann}}|v|\rangle$ the thermally averaged cross section times the relative velocity of χ and $\bar{\chi}$. We will use the expression provided in [8],

$$\langle \sigma_{\mathrm{ann}}|v|\rangle = \frac{1}{8\,T\,m_\chi^4\,K_2^2(x)} \int_{4m_\chi^2}^{\infty} \sqrt{s}\,\left(s - 4m_\chi^2\right) K_1(\sqrt{s}/T)\,\sigma_{\mathrm{ann}}\mathrm{d}s. \tag{3.17}$$

The Equation (3.16) describes the abundance in any temperature, may the species χ be coupled to the thermal bath or not, and it provides the "relic abundance" once χ decouples. We provide an example of the evolution of Y_χ in Figure 6.

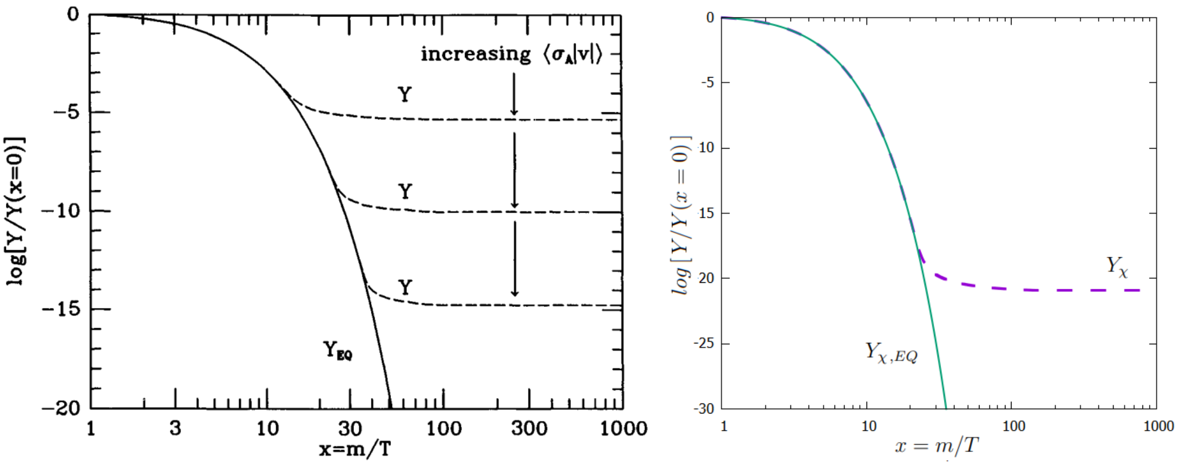

Figure 6: The freeze out of a massive particle species for different values of $\langle \sigma_{\rm ann}|v| \rangle$ [7] (left) and for the value of $\langle \sigma_{\rm ann}|v| \rangle$ that provides the abundance of DM observed today, $\Omega_{DM}h^2 \approx 0.12$ (right). The dashed line is the actual abundance, and the solid line is the equilibrium abundance.

At higher temperatures (low values of x) the abundance is the equilibrium one, with an exponential reduction at $T < m_\chi$, or in terms of x, $x < 1$ (this exponential reduction is showed in Equation (3.13)). Then, the decoupling occurs at lower temperatures for larger cross sections, which implies a lower relic density for the particle χ. The weaker the coupling of a WIMP, the earlier it decouples and the larger it is its final density.

$$\langle \sigma_{\rm ann}|v| \rangle \Downarrow \quad \Longrightarrow \quad \text{Time in equilibrium} \Downarrow \quad \Longrightarrow \quad Y_\infty \Uparrow . \tag{3.18}$$

We can see here that the only factor determining the relic abundance that we observe today, will be its interactions, specifically the value of $\langle \sigma_{\rm ann}|v| \rangle$.

On the other hand, it is convenient to relate Y_∞ (the value of Y today) with the density parameter for χ:

$$\Omega_\chi h^2 = \frac{\rho_\chi}{\rho_c} h^2 = \frac{m_\chi s_0}{\rho_c} h^2 \left(\frac{n_\chi}{s_0} \right) = \frac{m_\chi s}{\rho_c} Y_\infty = 2.75 \times 10^8 \, \frac{m_\chi}{\text{GeV}} Y_\infty . \tag{3.19}$$

This relation must be compared for a given WIMP model with the measured DM density in Equation (3.7). In Figure 6 (right) we represent the evolution of the abundance of the WIMP Y_χ. In particular, it provides $\Omega_\chi h^2 = 0.12$.

We would like to finish the section commenting on the so-called *WIMP miracle*. It turns out that a particle with weak couplings, with a cross section with the visible matter similar to the one provided by weak boson exchange, must have a mass of order 100 GeV to imply the *right* relic abundance. Larger masses would require stronger couplings, making the theory nonperturbative, whereas lower masses could make the particle invisible in direct searches. This hypothetical Weakly Interactive Massive Particle or WIMP would fulfil all the requirements to be a good DM candidate but can not be any of the particles of the Standard Model. This has motivated an intensive search for many decades. Unfortunately, all searches have been negative and it is becoming more and more difficult to define WIMP models not excluded by the data.

4 A WIMP model

The Higgs Portal

To define a model we need to specify the type of particle, its mass m_χ and its interactions (the mediator or "portal"). Our WIMP is a Majorana fermion[2] χ with a mass between 50 and 1000 GeV (see mass limitations in Equation (4.20)) and interactions with the visible matter mediated by the Higgs boson only, the so-called “Higgs Portal”. In addition, our model includes a second non-standard particle, a hypothetical heavy neutrino **N** that will imply a monochromatic signal at neutrino telescopes.

Let us follow an effective theory approach, assuming that the model is valid below a cutoff scale Λ and including higher dimensional operators. Since $\left(H^\dagger H\right)$ is one of the two lowest dimensional gauge invariant operators that one can write in the SM (the other one being the hyper-charge gauge field strength $B_{\mu\nu}$), one may expect that also $\left(H^\dagger H\right) - (dark\ sector)$ will be the lowest dimension operator connecting dark and visible sectors, which justifies the choice of the Higgs Portal [9]. More precisely, we can write two dim-5 operators:

$$Q_s = (H^\dagger H)(\bar{\chi}\chi)\,; \qquad Q_a = i(H^\dagger H)(\bar{\chi}\gamma_5\chi)\,, \tag{4.1}$$

where $H = (h^+\ h^0)$ is the Higgs doublet. In order to build the model, it may be more clear the use of two component-spinors of left handed chirality plus their conjugate[3]. The effective Lagrangian is just

$$-\mathscr{L}_{eff} = \frac{1}{2} m_\chi \chi\chi + \frac{c_s}{\Lambda} H^\dagger H \chi\chi - i\frac{c_a}{\Lambda} H^\dagger H \chi\chi + h.c. \tag{4.2}$$

with $c_{s,a}$ real. In four component notation (see footnote) this would correspond to

$$-\mathcal{L}_{eff} \supset \frac{1}{2} m_\chi \chi\chi + \frac{c_s}{\Lambda} Q_s + \frac{c_a}{\Lambda} Q_a\,. \tag{4.3}$$

[2] A gauge singlet fermion can be a Majorana field. In any case, our results for a Dirac fermion can be derived just by dividing by 2 or 4 (depending on the variable we are calculating).

[3] In this 2-component notation e_α and $e^c{}_\alpha$ are the electron and the positron both *left*, whereas their conjugate-contravariant $\bar{e}^{\dot{\alpha}}$ and $\bar{e}^{c\,\dot{\alpha}}$ define *right* spinors. The 4-component electron in the chiral representation of γ^μ is then $e = \begin{pmatrix} e_\alpha \\ \bar{e}^{c\,\dot{\alpha}} \end{pmatrix}$, while $\chi = \begin{pmatrix} \chi_\alpha \\ \bar{\chi}^{\dot{\alpha}} \end{pmatrix}$ is a 4-component (self-conjugate) Majorana fermion.

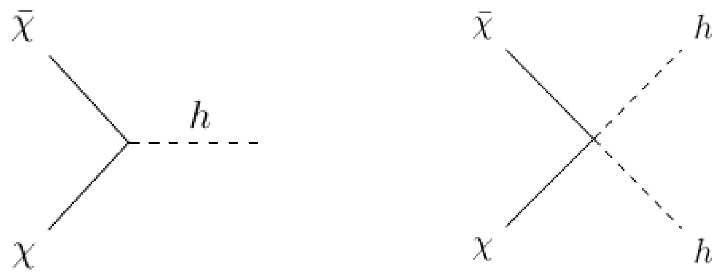

Figure 7: Vertices connecting χ with the Higgs boson h.

These operators may result after integrating out heavy particles. Note that the simultaneous presence of both couplings breaks parity. After electroweak symmetry breaking, the Higgs takes a vacuum expectation value (VEV). In the unitary gauge $H = \left(0,\ (h+\mathrm{v})/\sqrt{2}\right)$, and the Lagrangian becomes

$$-\mathscr{L}_{eff,\,DM} = \frac{1}{2}\,(m_\chi + \mathrm{v}^2)\,\chi\chi + \left[\frac{c_s}{\Lambda} - i\frac{c_a}{\Lambda}\right]\left(\frac{1}{2}h^2\chi\chi + \mathrm{v}h\chi\chi\right), \tag{4.4}$$

implying the vertices in Figure 7.

A heavy neutrino

The model also includes a heavy neutrino, a Dirac singlet (N, N^c) of similar mass m_N. Such fields are needed to give mass to the SM neutrinos through an inverse see-saw at the TeV scale. The relevant part of the Lagrangian at dim-5 (in 2-spinor notation) is just

$$-\mathscr{L}_{eff,\,N} \supset\ m_N\, NN^c + y_N\, HLN^c + \frac{c_N}{\Lambda} H^\dagger H\, NN^c + h.c.\,, \tag{4.5}$$

where $L = (\nu\ \ell)$ is a lepton doublet that we assume mostly along the τ flavor. After the Higgs takes the VEV the Lagrangian reads

$$-\mathscr{L}_{\rm eff}\ \supset\ m_N\, NN^c + \frac{y_N \mathrm{v}}{\sqrt{2}}\nu N^c + \frac{y_N}{\sqrt{2}}h\nu N^c + \frac{\mathrm{v}^2}{2}\frac{c_N}{\Lambda}NN^c + \frac{c_N}{\Lambda}\mathrm{v}hNN^c + \frac{c_N}{\Lambda}\frac{h^2}{2}NN^c. \tag{4.6}$$

This Lagrangian can be divided into two parts, the mass part and the interaction part. The first one reads

$$\begin{aligned} -\mathscr{L}_{\rm eff}\ &\supset\ m_N\, NN^c + \frac{y_N \mathrm{v}}{\sqrt{2}}\nu N^c + \frac{\mathrm{v}^2}{2}\frac{c_N}{\Lambda}NN^c\ = \\ &=\ \left(\left(\frac{y_N \mathrm{v}}{\sqrt{2}}\right)\nu + \left(M_N + \frac{\mathrm{v}^2}{2}\frac{c_N}{\Lambda}\right)N\right)N^c\,. \end{aligned} \tag{4.7}$$

Defining $m'_N = \sqrt{\left(M_N + \frac{\mathrm{v}^2}{2}\frac{c_N}{\Lambda}\right)^2 + \left(\frac{y_N \mathrm{v}}{\sqrt{2}}\right)^2}$ we obtain

$$-\mathscr{L}_{\rm eff} \supset m'_N\,(s_\alpha \nu + c_\alpha N)\,N^c = m'_N\, N' N^c\,, \tag{4.8}$$

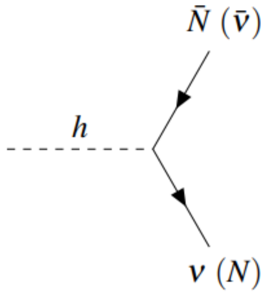

Figure 8: Vertex connecting the active and the sterile neutrinos with the Higgs boson.

with

$$s_\alpha = \frac{y_N \mathrm{v}}{\sqrt{2} m_N^{'}}\,, \tag{4.9}$$

and

$$\begin{cases} N^{'} = \quad c_\alpha N + s_\alpha \nu\,, \\ \nu^{'} = -s_\alpha N + c_\alpha \nu\,. \end{cases} \tag{4.10}$$

Notice that the active neutrino ν mixes with the sterile N but stay massless; the model can be completed with an inverse see saw to give mass to the standard neutrinos [10]. We will assume a mixing $s_\alpha \leq 0.1$.

Interactions

The interactions of the neutrino mass eigenstates are given by

$$\begin{aligned} -\mathscr{L}_{eff} \supset \left(\frac{y c_\alpha}{\sqrt{2}} - \frac{c_N}{\Lambda} \mathrm{v}\, s_\alpha\right) h\, \nu' N^c + \left(\frac{y s_\alpha}{\sqrt{2}} + \frac{c_N}{\Lambda} \mathrm{v}\, c_\alpha\right) h N' N^c + \\ + \left(\frac{c_N}{\Lambda}\frac{c_\alpha}{2}\right) h^2 N' N^c - \left(\frac{c_N}{\Lambda}\frac{s_\alpha}{2}\right) h^2 \nu' N^c\,. \end{aligned} \tag{4.11}$$

The first term describes the coupling of the Higgs to a sterile neutrino N and to an active neutrino ν (from now on we suppress the primes to indicate mass eigenstates). Combined with the Higgs coupling to χ, it will define the main connection between the dark and the visible matter. It is

$$-\mathscr{L}_{eff} \supset \frac{\tilde{y}_N}{\sqrt{2}}\, h\, \nu N^c\,, \tag{4.12}$$

with

$$\frac{\tilde{y}_N}{\sqrt{2}} = \left(\frac{m_N c_\alpha}{\mathrm{v}} - \frac{c_N \mathrm{v}}{\Lambda}\right) s_\alpha\,. \tag{4.13}$$

We show this vertex in Figure 8.

If $m_N < m_h = 125$ GeV, this coupling allows Higgs decays $h \to \nu \bar{N}$ with $\bar{N} \to \tau^+ W^-$ that have not been observed. Therefore, in that case we will require a value of $\tilde{y}_N$ giving a maximum branching ratio of 10% for this Higgs decay channel. More precisely, we will impose the following bounds:

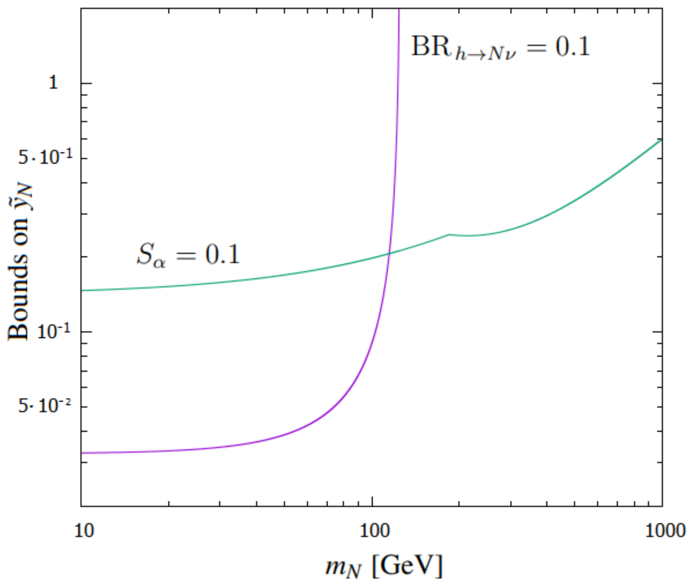

Figure 9: Maximum allowed value of $\tilde{y}_N$ imposed by each limitation, as a function of m_N.

i) For the scale of new physics Λ we take $\Lambda = 2m_\chi$, although for lower values of m_χ we take $\Lambda = \mathrm{v}$.

ii) The collider bounds on anomalous coupling to the weak bosons of ν_τ, now carrying a small sterile component, imply $s_\alpha \leq 0.1$ [11, 12]. We will then impose $S_\alpha \leq 0.1$. Using the definition of $\tilde{y}_N$ in Equation (4.13),

$$\tilde{y}_N \leq 0.14 \left(\frac{m'_N}{246\ \mathrm{GeV}} - 246\ \mathrm{GeV} \times \mathrm{Min}\left(\frac{1}{2m_\chi}, \frac{1}{246\ \mathrm{GeV}} \right) \right). \tag{4.14}$$

iii) The branching ratio of the Higgs to $\nu' + \bar{N} + \bar{\nu}' + N$ must be ≤ 0.1. Since

$$\Gamma_{h\to\nu'+\bar{N}} + \Gamma_{h\to\bar{\nu}'+N} = \frac{m_h^3}{32\pi} \left[\left(1 - \frac{m_N^2}{m_h^2}\right) \frac{\tilde{y}_N}{\sqrt{2}m_h} \right]^2, \tag{4.15}$$

and $\Gamma_{total} = 4.6^{+2.6}_{-2.5}$ MeV [13], we obtain

$$\tilde{y}_N \leq \frac{0.29\ \mathrm{GeV}^{1/2}}{m_h^{3/2}} \left(\frac{m_h}{1 - \frac{m_N^2}{m_h^2}} \right). \tag{4.16}$$

In Figure 9 we plot the maximum value of $\tilde{y}_N$ after imposing the two conditions above as a function of m_N. From now on in this work we will take the maximum value of $\tilde{y}_N$ consistent by both restrictions.

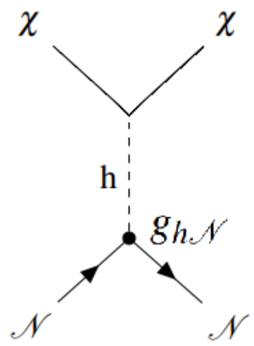

Figure 10: Elastic interaction between a DM particle χ and a nucleon $\mathcal{N}$.

To sum up, our model includes 6 parameters: the mass m_χ of the the DM particle; the two couplings $c_{s,a}/\Lambda$ connecting χ with the Higgs; the mass m_N of a heavy Dirac neutrino (N, N^c); the heavy-light Yukawa $\tilde{y}_N$ and the mixing s_α of this heavy neutrino with the active ones, with the relation $\tilde{y}_N \approx s_\alpha m_N/v$ possibly broken by a dim-5 operator.

Elastic DM-Nucleon cross section and direct detection

As we mentioned before, direct search experiments try to see the recoil of a heavy nucleus hit by a dark matter particle, a process that depends on the DM-nucleon elastic cross section. In our model this process is mediated by a Higgs in the t channel, as shown in Figure 10.

The Higgs boson couples to the quarks and (through heavy quark loops) to the gluons in the nucleon, inducing a Higgs-nucleon Yukawa coupling $g_{h\mathcal{N}}$ that is usually parameterized [14, 15] as $g_{h\mathcal{N}} = f_\mathcal{N} m_\mathcal{N}/\mathrm{v}$, with $m_\mathcal{N} = 0.94$ GeV and $f_\mathcal{N} = 0.30$. This implies an elastic DM-nucleon cross section mediated by the Higgs in the t-channel that is spin-independent (insensitive to the spin of the nucleon)

$$\sigma(\chi\mathcal{N} \to \chi\mathcal{N}) = \frac{4}{\pi}\,\frac{c_s^2 + c_a^2\beta^2}{\Lambda^2}\left(\frac{\mu_\mathcal{N}\, m_\mathcal{N}\, f_\mathcal{N}}{m_h^2}\right)^2, \tag{4.17}$$

with $\mu_\mathcal{N} = m_\mathcal{N} m_\chi/(m_\mathcal{N} + m_\chi)$. The experiment XENON1T has obtained bounds on $\sigma^{\mathrm{SI}}_{\chi\mathcal{N}}$ for m_χ between 10 GeV and 10 TeV [16], that we fit with the approximate expression

$$\sigma^{\mathrm{SI,max}}_{\chi\mathcal{N}} \leq 0.9\times 10^{-48}\, m_\chi^{1+169/m_\chi^2}\ \mathrm{cm}^2, \tag{4.18}$$

with m_χ in GeV. These bounds imply a maximum value of

$$\frac{c_s}{\Lambda} \leq \frac{c_s^{\max}}{\Lambda} = 2.5\times 10^{-6}\,\frac{0.94 + m_\chi}{\sqrt{m_\chi^{1-169/m_\chi^2}}}\ \mathrm{GeV}^{-1}. \tag{4.19}$$

However, they do not constrain significantly the coupling c_a. The reason is that the typical velocity of the DM particles trapped in our galaxy is around 300 km/s, and the c_a contribution in the expression above appears suppressed by a factor of $\beta^2 \approx 10^{-6}$.

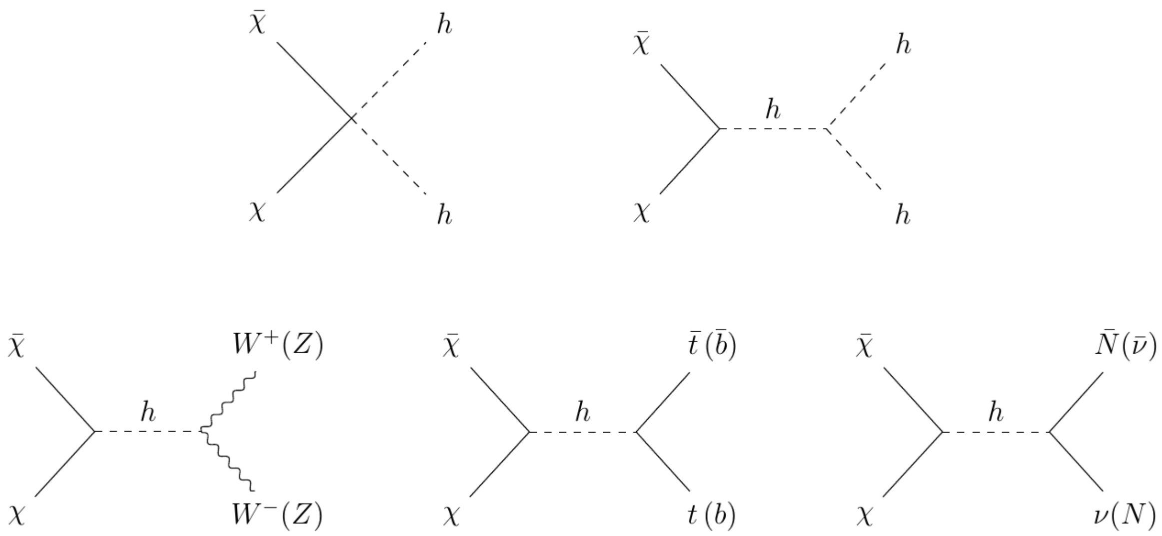

Figure 11: Leading diagrams in DM annihilation.

Annihilation cross section

The DM annihilation processes $\chi\bar{\chi} \to X$, with X any lighter particle (or particles), will determine the relic abundance of our WIMP and also the neutrino signal from the Sun. In our model the most significant diagrams mediating this annihilation are given in Figure 11.
Looking at the diagrams of Figure 11 we make two important observations:

i) LEP has observed the Z decay and fits perfectly with the SM prediction, so we will not allow Z decays into $N\nu$. This forbids values of m_N below M_Z. By contrast, if the annihilation channel $\chi\bar{\chi} \to N\nu$ is open, this implies that $m_\chi > m_Z/2$. Throughout the analysis we will take:

$$\begin{cases} m_\chi \geq 50 \text{ GeV}\,, \\ m_N \geq 100 \text{ GeV}. \end{cases} \tag{4.20}$$

ii) By simple kinematic, a DM annihilation at $s \approx 4m_\chi^2$ (as it may happen in the Sun) the channel $\chi\bar{\chi} \to \bar{N}\nu$ will produce an active neutrino of energy

$$E_\nu = m_\chi \left(1 - \frac{m_N^2}{4m_\chi^2}\right). \tag{4.21}$$

A signal of monochromatic neutrinos could be searched for at neutrino telescopes, as KM3NeT.

We have calculated all these annihilation channels; the result can be written as

$$\sigma_{\rm ann} = \frac{1}{4\pi\Lambda^2} \frac{c_s^2\left(1-\frac{4m_\chi^2}{s}\right)+c_a^2}{\sqrt{1-\frac{4m_\chi^2}{s}}} f(m_\chi) \approx \frac{1}{4\pi\Lambda^2\beta}\left(c_s^2\beta^2+c_a^2\right) f(m_\chi)\,, \tag{4.22}$$

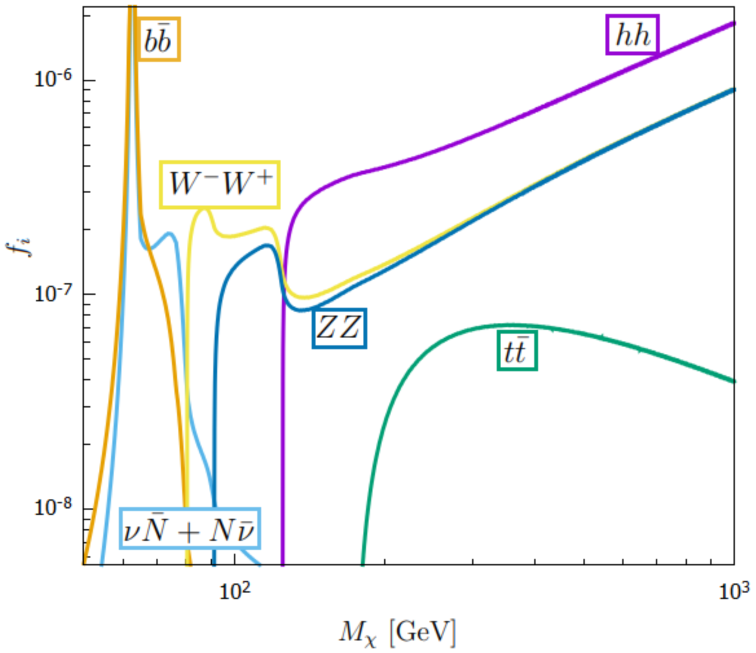

Figure 12: Value of f_i for the different annihilation channels as a function of m_χ. It can be seen here the relative frequency between the different annihilation channels.

where β is the velocity of χ in the center of mass frame (the approximation corresponds to the non-relativistic limit) and $f(m_\chi)=\sum_i f_i$ gives the contribution of the different channels opened at a given value of m_χ. The different f_i are [9]

$$\begin{aligned}
f_h &= \left(1+\frac{3m_h^2}{s-m_h^2}\right)\sqrt{1-\frac{4m_h^2}{s}}\,,\\
f_Q &= \frac{3m_Q^2}{s-m_h^2}\,\frac{s-4m_Q^2}{s-m_h^2}\sqrt{1-\frac{4m_Q^2}{s}}\,,\\
f_V &= \frac{2m_V^4}{(s-m_h)^2}\left[2+\left(1-\frac{s}{2m_V^2}\right)^2\right]\sqrt{1-\frac{4m_V^2}{s}}\,,\\
f_N &= \frac{\tilde{y}_N^2 v^2}{2\left(s-m_h^2\right)}\,\frac{s-m_N^2}{s-m_h^2}\left(1-\frac{m_N^2}{s}\right)\,,
\end{aligned} \tag{4.23}$$

with $Q=t,b$ and $V=Z,W$. Attention should be paid when reading [9], because there is

a missing factor of 3 (number of quark colors) in f_Q. In addition, [9] do not consider the channels W^+W^- and ZZ, that turn out to be very significant.
In Figure 12 we plot the factors f_i for different values of m_χ and taking $m_N = 1.4 m_\chi$, a relative mass that opens the channel $\chi\bar{\chi} \to \nu N$. The figure reveals some interesting features:

i) For $m_\chi \gg m_t$ the dominant annihilation channel is $\chi\bar{\chi} \to hh$. In particular, for this range, $\chi\bar{\chi} \to hh$ has a BR of 0.5 approximately.

ii) At low values of m_χ, DM goes predominantly to $b\bar{b}$ and $(\nu\bar{N}, N\bar{\nu})$.

Value of $\mathbf{c_s/\Lambda}$ and $\mathbf{c_a/\Lambda}$

The two free parameters c_s/Λ and c_a/Λ will be fixed in the following way for each value of m_χ that we consider. For c_s/Λ we will use the maximum value allowed by direct searches, which is c_s^{max}/Λ given by the Equation (4.19).
Notice that the contribution of c_s/Λ to the elastic cross section is suppressed by a factor of $\beta^2 \approx 10^{-6}$ and is therefore unconstrained. In contrast, in the annihilation cross section, it is the contribution of c_s/Λ the one suppressed by a factor of $\beta^2 \approx (1/20)^2$ (approximated value of β^2 during freeze out).Then, it will be c_a/Λ the one dictating the relic density.

Therefore, in order to know c_a/Λ we go back to the results in Section 3. We have created a program that solves the differential equation in (3.16) and gives Y_∞ (and $\Omega_{DM}h^2$) for any value of c_s/Λ and c_a/Λ. We have introduced the value of $c_s/\Lambda = c_s^{max}/\Lambda$ and have varied c_a/Λ until $\Omega_{DM}h^2 \approx 0.12$ is the one predicted. In Figure 13 we plot the values of c_a/Λ and c_s/Λ obtained for every possible value of m_χ, for $m_N = 1.4 m_\chi$,

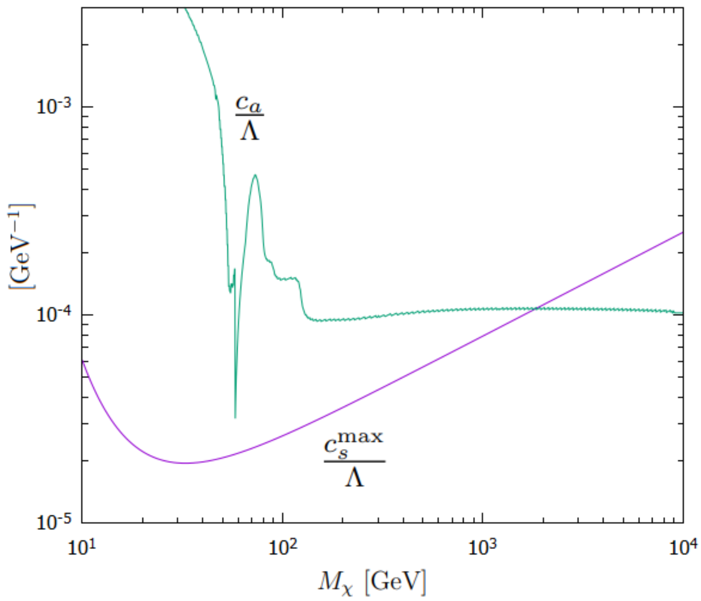

Figure 13: Values of c_a/Λ and c_s/Λ as a function of m_χ, taking $m_N = 1.4 m_\chi$. We take $c_s/\Lambda = c_s^{max}/\Lambda$, and c_a/Λ is fixed in order to predict $\Omega_{DM}h^2 \approx 0.12$.

5 Indirect signal at neutrino telescopes

Capture of DM by the Sun

The DM is distributed in the Galactic Halo. The DM particles do not orbit coherently like the gas and the stars in our galaxy, but each particle has a different random direction and the average velocity is zero $\langle \vec{v}_{DM} \rangle = 0$. This is illustrated in Figure 14. Since DM, on average, does not move respect to the galaxy, as the Sun moves, it will see a DM wind with $\langle \vec{v}_{DM} \rangle = 220$ km/s and $\langle v_{DM} \rangle \approx 300$ km/s.

As the wind of DM particles passes through the Sun first it accelerates due to the gravitational fall, but once there some of the particles may interact with a solar nucleus and lose velocity in the collision. If this final velocity is below the escape velocity of the Sun at the point of the collision, it will be trapped and slowly will end up near the center.

The DM particles will then accumulate, and as their density grows it will be more likely that two of them find each other and annihilate. If the products of the annihilation include neutrinos, they could escape the Sun and reach the Earth. This is actually the final goal of our analysis, to determine whether this model may produce a neutrino signal from DM annihilation observable at a neutrino telescope.

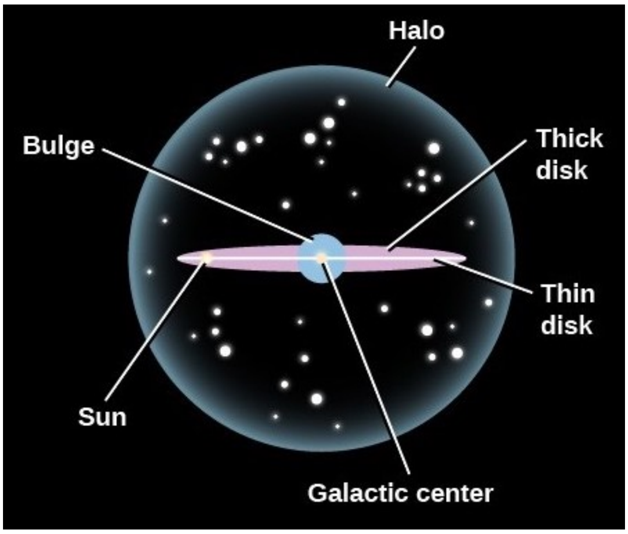

Figure 14: Scheme of the sun rotating around the DM halo [2].

DM annihilation rate in the Sun

As more and more particles of DM are trapped by the Sun, the annihilation rate Γ_A will increase. After enough time, there will be a moment in which the particles annihilate at the same rate that they are captured, *i.e.*, the system tends to a stationary regime where the rate of annihilations is only dictated by the capture rate C, and both the number of trapped DM particles and the neutrino flux that they produce remain constant. More precisely, in that regime the annihilation rate is $\Gamma_A = C/2$, where the 2 factor accounts the fact that one annihilation requires the capture of two DM particles.

However, we need to make sure that the system has reached the stationary regime. If it has not been reached, Γ_A will be less than $C/2$. In [17, p.293] it is shown that the annihilation rate at any given time is

$$\Gamma_A = \frac{C}{2}\tanh^2\left(\frac{t}{\tau}\right), \tag{5.1}$$

where τ is the required time to reach stationary regime. In particular, we want to estimate whether the age of the Sun, $t_\odot$, is smaller than τ or not. For the sun [17, p.294] it is

$$\frac{t_\odot}{\tau} \approx 330\left(\frac{C_\odot}{\mathrm{s}^{-1}}\right)^{1/2}\left(\frac{\langle\sigma_{\mathrm{ann}}\beta\rangle}{\mathrm{cm}^3\,\mathrm{s}^{-1}}\right)^{1/2}\left(\frac{m_\chi}{10\,\mathrm{GeV}}\right)^{3/4}, \tag{5.2}$$

where the suppression factor $\tanh^2(t/\tau)$ takes into account whether the stationary regime has been reached yet.
To obtain $t_\odot/\tau$ in our model we need to calculate:

i) **The capture rate**, defined as $C = \mathrm{d}N_\chi^{\mathrm{cap}}/\mathrm{d}t$. It can be obtained from the same elastic cross sections from direct searches that were described before, in Figure 10. We will adapt the results obtained in Equation (4.17) to the elastic cross section between the solar nuclei and the DM particles around the Sun. Then, the capture rate will be determined only by c_s/Λ.

   First we deduce the elastic cross section with the different solar nuclei, using the nuclear response functions in [18]. In particular, we will include the collisions with the 6 most abundant nuclei (H, He, N, O, Ne, Fe) in the Sun. We will use the AGSS09 solar model [19] and the SHM^{++} velocity distribution of the galactic DM [20]. We include the thermal velocity for the solar nuclei, although their net effect is not important (*e.g.*, at $m_\chi = 100$ GeV it increases a 5% the capture rate by solar hydrogen but reduces in a 40% the one by iron, and both effects cancel). For $m_\chi \geq 10$ GeV and a maximum coupling $c_s^{\max}/\Lambda$ we fit the capture rate of the sun to

$$C_\odot^{\max} \approx 2.30\times 10^{21}\, m_\chi^{-1-\frac{22}{m_\chi}+\frac{240}{m_\chi^2}}\ \mathrm{s}^{-1}, \tag{5.3}$$

   where m_χ is expressed in GeV. We have represented this capture rate as a function of m_χ in Figure 15.

ii) **The thermally averaged cross section** $\langle\sigma_{\mathrm{ann}}\beta\rangle$. In Equation (4.22) we see that σ_{ann} is proportional to β^{-1}, what simplifies the calculation of this thermal average. For our model we obtain

$$\langle\sigma_{\mathrm{ann}}\beta\rangle = 3.89\times 10^{-28}\,\frac{c_a^2}{4\pi\Lambda^2}\,f(m_\chi)\ \mathrm{GeV}^2\mathrm{cm}^3\,\mathrm{s}^{-1}. \tag{5.4}$$

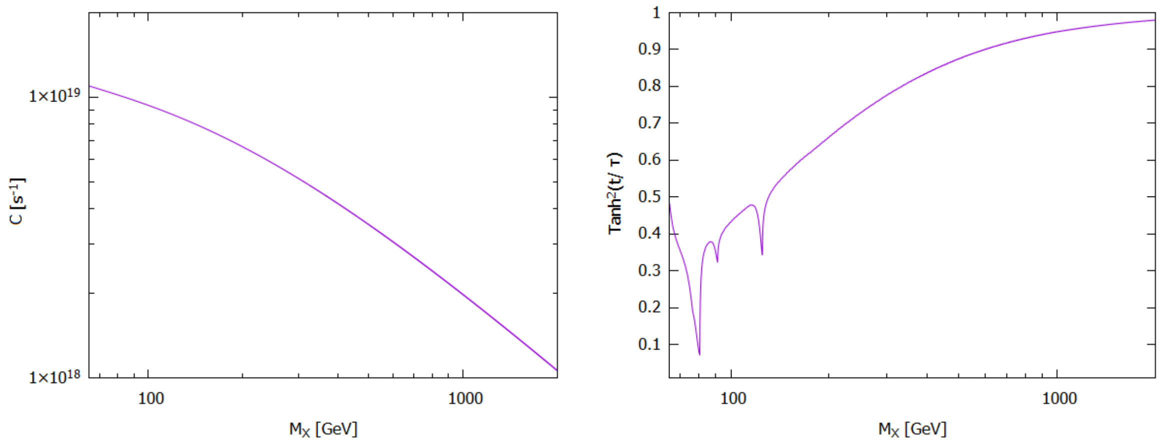

Figure 15: Capture rate of the sun $C_\odot$ (left) and suppression factor $\tanh^2\left(\frac{t_\odot}{\tau}\right)$ (right) as a function of m_χ.

Using the values of c_s/Λ and c_a/Λ required by the relic abundance, we obtain the value of the suppression factor $\tanh^2\left(\frac{t}{\tau}\right)$ that must multiply the capture rate (both in Figure 15) to deduce the DM annihilation rate in the Sun.

Neutrino flux reaching the Earth

To obtain the neutrino flux from DM annihilation in the Sun that reaches the Earth, we have to include

i) **The neutrino yield** (distribution of neutrinos $\mathrm{d}N_\nu/\mathrm{d}E$) produced per annihilation, f_ν. Each annihilation channel gives a different yield, that has to be multiplied by the frequency of the channel to obtain the total neutrino yield.

ii) **The annihilation rate**: We need to know how many annihilations occur per unit of time, *i.e.*, the value of Γ_A given in Figure 15.

iii) **The area factor**: The neutrinos produced in the Sun will exit in all directions with equal probability. Since they will be distributed in the area of a sphere with radius the distance Sun-Earth D_{SE} , the flux (number of neutrinos per unit area) is obtained dividing the yield by $4\pi D_{SE}^2$.

Combining all these elements, the neutrino flux from DM annihilation received on Earth is just

$$\frac{dN_\nu}{dt\ \ dE\ \ dS} = f_\nu(E)\,\frac{C_\odot}{2}\tanh^2\left(\frac{t}{\tau}\right)\frac{1}{4\pi D_{SE}^2}. \tag{5.5}$$

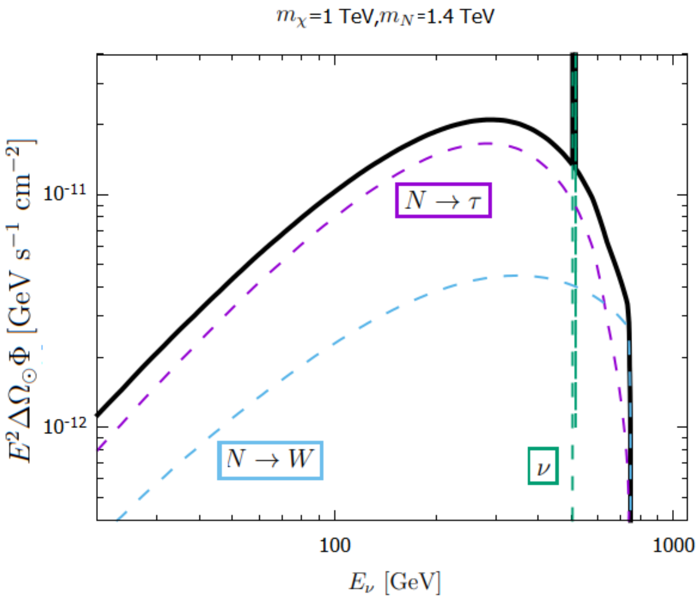

Figure 16: Different contributions of the channel $\chi\bar{\chi}\to N\bar{\nu}+\bar{N}\nu$ to the neutrino flux compared with the total flux from the channel, for the case $m_\chi = 1$ TeV, $m_N = 1.4$TeV .

Yields

We obtain the neutrino yields after the propagation from the Sun to the Earth for each annihilation channel with the $\chi arov$ software [21]. The channels $\chi\bar{\chi}\to N\bar{\nu}(\bar{N}\nu)$ and $\chi\bar{\chi}\to hh$, not included in $\chi arov$, require some elaboration.

i) $\chi\bar{\chi}\to \mathbf{N}\bar{\nu}(\bar{\mathbf{N}}\nu)$: We add the contribution due both to the active neutrino and to the heavy neutrino.

   a) The active neutrino is monochromatic, the yield gives a peak of total area equal to one. The width of this peak will be limited by experimental error, but we will take the one corresponding to 100 bins for each yield (the width of the bin is the energy range divided by 100).

   b) The heavy neutrino is mildly relativistic, with energy $E_N = m_\chi\left(1+\frac{m_N^2}{4m_\chi^2}\right)$, and will decay in τ and W. The W will exit with an approximate energy $E_W = 0.5\,E_N\left(1+\frac{m_W^2}{m_N^2}\right)$, while the τ will take the remaining energy in E_N. We then use $\chi arov$ to obtain the energy distribution of the neutrinos originated from such W and τ lepton.

   In Figure 16 we represent each contribution to the $\chi\bar{\chi}\to N\bar{\nu}+\bar{N}\nu$ yield.

ii) $\chi\bar{\chi}\to \mathbf{hh}$: $\chi arov$ provides the neutrino distribution for Higgs decays into SM particles only. However, we allow the decays $h\to N\bar{\nu}+\bar{N}\nu$ with a 10% branching ratio. We then

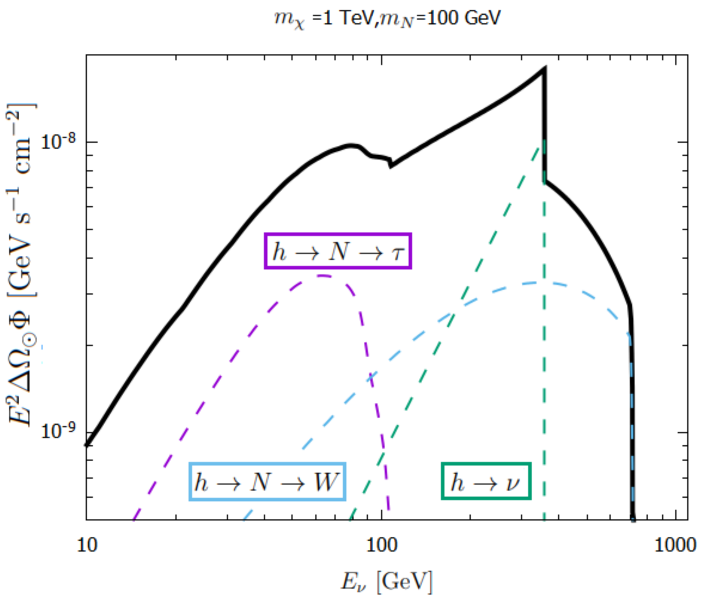

Figure 17: Different contributions of the channel $\chi\bar{\chi} \to hh$ to the neutrino flux compared with the total flux from the channel, for the case $m_\chi = 1$ TeV, $m_N = 100$ GeV .

multiply by 0.9 the yield obtained for $\chi\bar{\chi} \to hh$ by $\chi arov$, and add the new decay channel.

We proceed like in the previous case but adapting the energies of both the active and the heavy neutrinos resulting from the Higgs decay. In particular, it is easy to see that the active neutrino exits with a flat energy distribution between

$$\begin{cases} E_{min} = \dfrac{m_\chi\left(m_h^2 - m_N^2\right)}{2m_h^2}\left(1 - \sqrt{1 - \left(\dfrac{m_h}{m_\chi}\right)^2}\right), \\ E_{max} = \dfrac{m_\chi\left(m_h^2 - m_N^2\right)}{2m_h^2}\left(1 + \sqrt{1 - \left(\dfrac{m_h}{m_\chi}\right)^2}\right). \end{cases} \tag{5.6}$$

The area of this yield must be 0.2, as 10% of the times each one of the two Higgs bosons from $\chi\bar{\chi}$ go through this channel.

In Figure 17 we represent the different fluxes of neutrinos originated through the $\chi\bar{\chi} \to hh$ channel.

Neutrino Background

In our neutrino telescope we will observe neutrinos in addition to the possible flux created by the DM annihilation. In particular, if we point to a "fake Sun" (a region in the sky with the angular size of the Sun but no actual Sun) we will see the atmospheric neutrino background.

If we point to the Sun we will also see neutrinos even if there is no DM: the ones produced when high energy cosmic rays shower in the Sun's surface. We will use the expressions in [22] for both backgrounds.

For the atmospheric background we integrate over a solid angle $\Delta\Omega_\odot$ that corresponds the Sun seen from Earth , a circle of 0.26° radius, and we add the muon and electron neutrino flavors

$$\Delta\Omega_\odot \Phi^{\rm atm}(E,\theta) = \Delta\Omega_\odot \Phi^{\rm atm}_{\nu_\mu}(E,\theta) + \Delta\Omega_\odot \Phi^{\rm atm}_{\nu_e}(E,\theta). \tag{5.7}$$

with

$$\begin{aligned} \Delta\Omega_\odot \Phi^{\rm atm}_{\nu_\mu}(E,\theta) =& 4.42\times 10^{-6}\ E^{-2.97-0.0108\,log(E)-0.00141\,log^2(E)}\ F_1^{\rm atm}(E,\theta)\,,\\ \Delta\Omega_\odot \Phi^{\rm atm}_{\nu_e}(E,\theta) =& 1.94\times 10^{-6}\ E^{-3.30-0.0364\,log^{1.35}(E)+0.0103\,log^{1.85}(E)}\ F_2^{\rm atm}(E,\theta) \end{aligned} \tag{5.8}$$

and

$$F_1^{\rm atm}(E,\theta) = \frac{\left(\frac{176}{E}\right)^{0.6} + cos[\theta^*\left(\frac{\theta}{4}\right)]}{\left(\frac{176}{E}\right)^{0.6} + cos[\theta^*\left(\theta_z\right)]}; \quad F_2^{\rm atm}(E,\theta) = \frac{\left(\frac{7.5\times10^{-4}}{E}\right)^{0.21} + cos[\theta^*\left(\frac{\theta}{4}\right)]}{\left(\frac{7.5\times10^{-4}}{E}\right)^{0.21} + cos[\theta^*\left(\theta_z\right)]}, \tag{5.9}$$

being $\theta^*(\theta_z)$ defined as

$$\tan\ \theta^* = \frac{R_\oplus sin\ \theta_z}{\sqrt{R_\oplus^2 cos^2\theta_z + (2R_\oplus + h)h}}\,. \tag{5.10}$$

For the neutrinos from the solar disk, we have to add several components: neutrinos produced in the Sun surface (they come in the three flavors with the same frequency); neutrinos produced when neutrons also produced in the Sun reach the Earth and shower in the atmosphere; and the atmospheric neutrinos produced by cosmic rays coming form the Sun direction (the cosmic ray shadow of the Sun is not complete),

$$\Delta\Omega_\odot \Phi^\odot(E,t) = 3\ \Delta\Omega_\odot \Phi^\odot_{\nu_i}(E,t) + \Delta\Omega_\odot \Phi^{shad+n}_{\nu_\mu}(E,t) + \Delta\Omega_\odot \Phi^{shad+n}_{\nu_e}(E,t)\,, \tag{5.11}$$

where t is expressed in years and takes into account the 11-year solar cycle ($t=0$ at a solar minimum). The 3 contributions are

$$\begin{cases} \Delta\Omega_\odot \Phi^\odot_{\nu_i}(E,t) = \left(6.32\times10^{-9} - \dfrac{2.43\times10^{-6} sin^2(\frac{\pi t}{11})}{900+E}\right) E^{-1.20-0.1 log(E)-0.0042\,log^2(E)+1.6\times10^{-5} log^4(E)} \\ \Delta\Omega_\odot \Phi^{shad+n}_{\nu_\mu}(E,\theta,t) = 4.38\times10^{-6} E^{G_1^{shad+n}} F_1^{\rm atm}(E,\theta) \\ \Delta\Omega_\odot \Phi^{shad+n}_{\nu_\mu}(E,\theta,t) = 1.38\times10^{-6} E^{G_2^{shad+n}} F_2^{\rm atm}(E,\theta) \end{cases}, \tag{5.12}$$

with

$$
\begin{aligned}
G_1^{shad+n}(E,t) =& -2.98 - 0.017log(E) + 0.012cos\left(\frac{2\pi t}{11}\right) log^2(E) \\
& -3.3\times10^{-4}log^3(E) - 4.1\times10^{-6}log^5(E)\,, \\
G_2^{shad+n}(E,t) =& -3.1 - 0.061log(E) - 5.3\times10^{-7}log^6(E) \\
& -cos\left(\frac{2\pi t}{11}\right)\left(0.00305\,log(E) + 2.1\times10^{-6}log^5(E)\right)\,.
\end{aligned}
\tag{5.13}
$$

We will take the Sun at a zenith angle of $\theta = +45^\circ$ and solar activity will be averaged between the maximum and a minimum activity within the solar cycle.

6 Final results

Let us discuss the neutrino fluxes that reach a neutrino telescope for several benchmark values of m_χ and m_N.

$m_\chi = 70$ GeV, $m_N = 100$ GeV

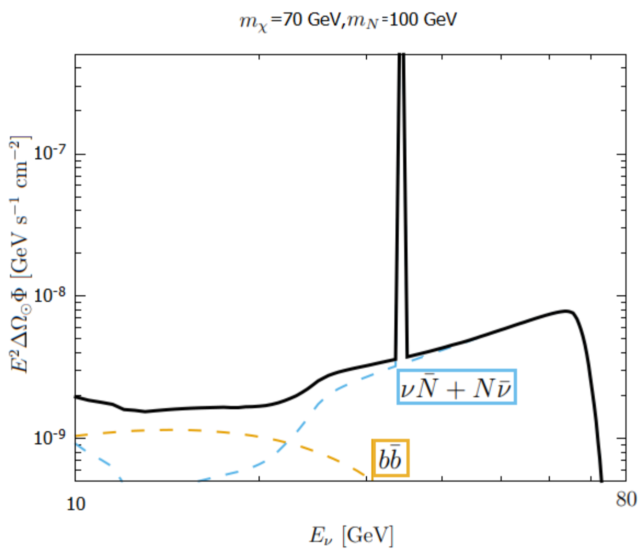

Figure 18: Contribution of each annihilation channel to the total neutrino flux from DM for $m_\chi = 70$ GeV, $m_N = 100$ GeV.

Here there are only two open annihilation channels, bb and $N\nu$, that we plot in Figure 12. We see that the heavy neutrino channel dominates, although the DM flux is below the background, as shown in Figure 18. The monochromatic peak in the spectra, however, is over the background for a narrow region over 35 GeV, as we can see in Figure 19. This could offer some hope in searches at neutrino telescopes.

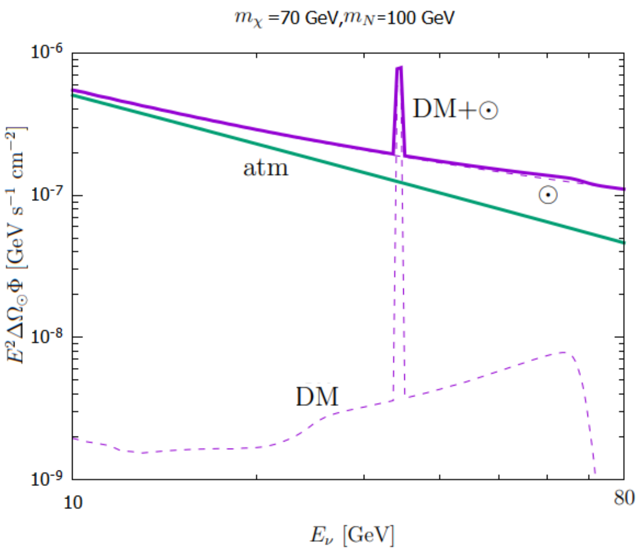

Figure 19: Neutrino Flux from DM and backgrounds from the Sun and from a "fake Sun" for $m_\chi = 70$ GeV, $m_N = 100$ GeV.

$m_\chi = 1$ TeV, $m_N = 1.4$ TeV

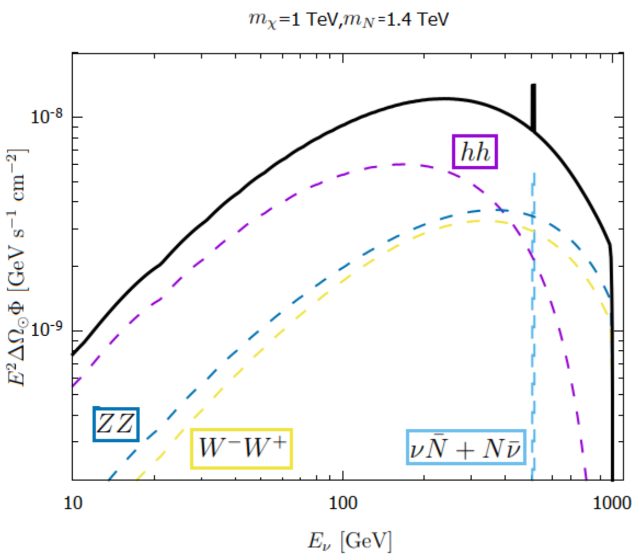

Figure 20: Contribution of each annihilation channel to the total neutrino flux from DM for $m_\chi = 1$ TeV, $m_N = 1.4$ TeV.

For this large value of m_χ all the annihilation channels are open. In Figure 12 we see the relevance of each one: hh, ZZ, and W^-W^+ dominate as they have the larger branching ratios. In this case, the monochromatic neutrinos will contribute less than for $m_\chi = 70$ GeV because the frequency of the $N\nu$ is lower, giving a weaker peak. Despite this, it is still significant, as shown in Figure 20.

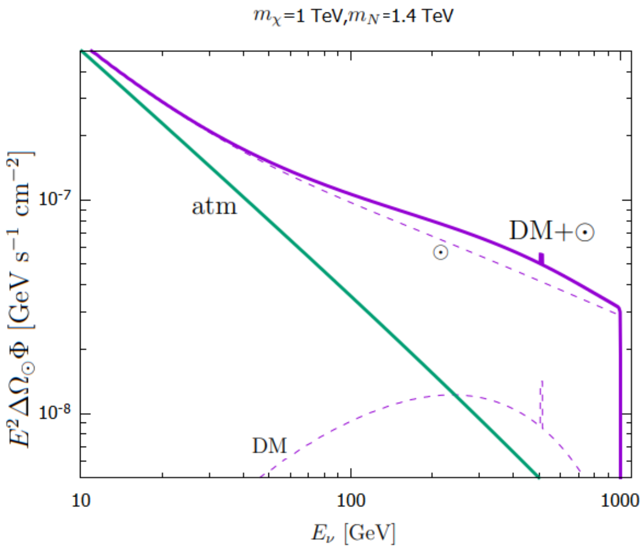

Figure 21: Neutrino Flux from DM and backgrounds from the Sun and from a "fake Sun" for the case $m_\chi = 1$ TeV, $m_N = 1.4$ TeV.

$m_\chi = 1$ TeV, $m_N = 100$ GeV

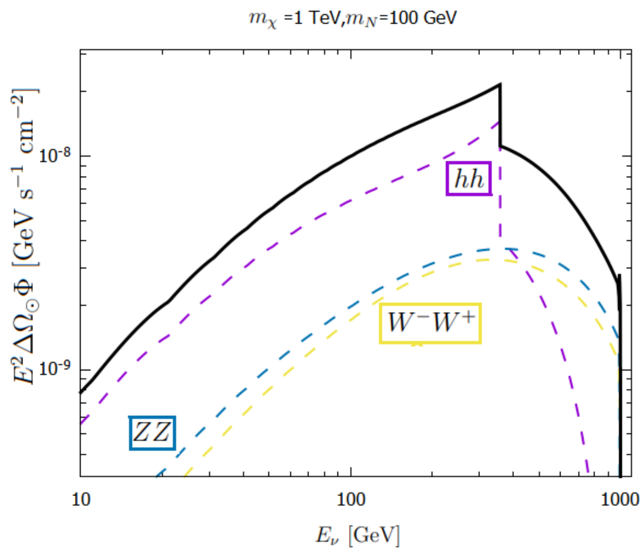

Figure 22: Contribution to the neutrino flux of each annihilation channel in comparison with the total neutrino flux from DM, for the case $m_\chi = 1$ TeV, $m_N = 100$ GeV.

The difference here with the previous case is that, being $m_N < m_h$, the Higgs boson resulting from DM annihilation can decay into νN. As we see in Figure 22, this provides a kind of peak-like feature caused by the ν from this decay (see Figure 17). This new contribution is the most important one.

Note also that for $m_N << m_\chi$ the frequency of the annihilation channel $N\nu$ will be far smaller and the truly monochromatic peak is negligible.

In Figure 23 we see the total DM signal characteristic shape versus the background, a flux that could be interesting at neutrino telescopes.

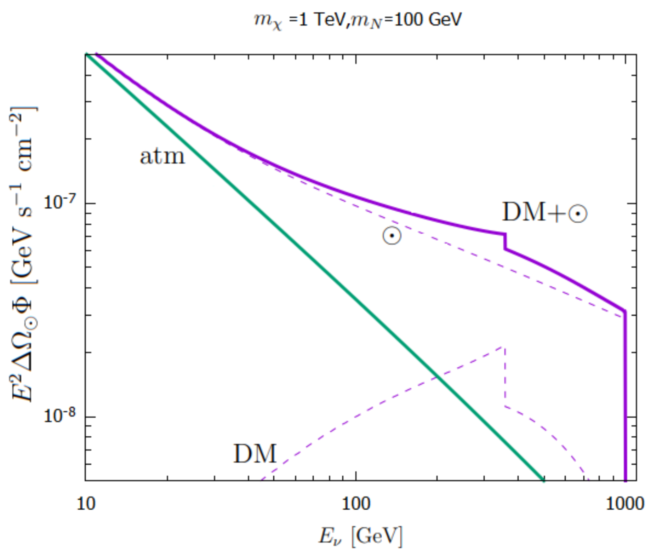

Figure 23: Neutrino Flux from DM in comparison with the backgrounds from the sun and from the atmosphere for the case $m_\chi = 1$ TeV, $m_N = 100$ GeV.

7 Conclusions

In this Master Thesis we have studied a model for the dark matter of the Universe. The work involves aspects from different branches of physics, from particle physics and gravitation to thermodynamics.

First we have discussed how cosmology can explain the abundance of DM that we observe today. Along the way, we have been studied topics related to the expansion of the Universe or the evolution of the different particle species in the early Universe.
Then we have proposed a WIMP model and have explored its particle physics implications. To do that, we have used concepts from effective field theories and quantum field theory.
Finally, we have studied in detail the possible signal that the model could imply at a neutrino telescope, getting familiar with the bounds imposed by direct search experiments like

XENON1T and learning some basic concepts in experimental physics.

In conclusion, I would say that this has been the perfect activity to do while attending the Master's lessons. In the different courses of the Master I have learned concepts that later I have applied here, getting a clear idea of their meaning, and learning that they are actually useful. But, at the same time, this thesis has been a motivation to go deeper with the contents in the Master.

The Master's thesis has also been a good introduction to real research in physics. During the thesis I have read a lot of papers and I have dealt with real research issues, like throwing away results when they are not "interesting" or change the hypothesis to get them interesting.

I also have learned that one has to be very carefully: this is not an exam and nobody knows the final result in advance. A little mistake might lead you to a useless waste of time and effort. Of course, nobody wants to publish a work with mistakes, if someone else detects them you might lose credibility in scientific community.

The work done has been worth and we are confident that the results obtained are consistent. To decide whether this kind of signal might be observable at, for example, KM3NeT would require a more dedicated analysis, that could be attempted. DM is a mistery that has occupied physicists for decades, and monochromatic neutrinos are an interesting possibility difficult to achieve.

Finally, to mention that following these results, we are preparing a paper that we hope to have ready in a few weeks.

References

[1] B. Hubert and P. Alan. "Modeling Wave Dark Matter in Dwarf Spheroidal Galaxies". In: *Journal of Physics: Conference Series* 2 (Jan. 2013). DOI: 10.1088/1742-6596/615/1/012001.

[2] J. Romero Gomez. *Mirando al joven universo: descubrimiento de 9 lentes gravitacionales nuevas*. 2020. URL: https://astrobitos.org/2020/01/08/mirando-al-joven-universo-descubrimiento-de-9-lentes-gravitacionales-nuevas/.

[3] A. Casas. *La luz del origen del universo*. Arbor, 2015.

[4] N. Aghanim et al. "Planck 2018 results. VI. Cosmological parameters". In: *Astronomy &amp Astrophysics* 641 (Sept. 2020), A6. DOI: 10.1051/0004-6361/201833910. URL: https://doi.org/10.1051%2F0004-6361%2F201833910.

[5] James M. Cline. *TASI Lectures on Early Universe Cosmology: Inflation, Baryogenesis and Dark Matter*. 2021. arXiv: 1807.08749 [hep-ph].

[6] Lars Husdal. "On Effective Degrees of Freedom in the Early Universe". In: *Galaxies* 4.4 (Dec. 2016), p. 78. DOI: 10.3390/galaxies4040078. URL: https://doi.org/10.3390%2Fgalaxies4040078.

[7] Michael S. Turner Edward W. Kolb. *The early universe*. Frontiers in Physics. Addison-Wesley Publishing Company, 1990. ISBN: 0201116030.

[8] Mirco Cannoni. "Relativistic and nonrelativistic annihilation of dark matter: a sanity check using an effective field theory approach". In: *The European Physical Journal C* 76.3 (Mar. 2016). DOI: 10.1140/epjc/s10052-016-3991-2. URL: https://doi.org/10.1140%2Fepjc%2Fs10052-016-3991-2.

[9] Laura Lopez-Honorez, Thomas Schwetz, and Jure Zupan. "Higgs portal, fermionic dark matter, and a Standard Model like Higgs at 125 GeV". In: *Physics Letters B* 716.1 (Sept. 2012), pp. 179–185. DOI: 10.1016/j.physletb.2012.07.017. URL: https://doi.org/10.1016%2Fj.physletb.2012.07.017.

[10] G. Hernández-Tomé, J. I. Illana, and M. Masip. "The ρ parameter and $H^0 \to l_i l_j$ in models with TeV sterile neutrinos". In: *Physical Review D* 102.11 (Dec. 2020). DOI: 10.1103/physrevd.102.113006. URL: https://doi.org/10.1103%2Fphysrevd.102.113006.

[11] Enrique Fernandez-Martinez, Josu Hernandez-Garcia, and Jacobo Lopez-Pavon. "Global constraints on heavy neutrino mixing". In: *Journal of High Energy Physics* 2016.8 (Aug. 2016). DOI: 10.1007/jhep08(2016)033. URL: https://doi.org/10.1007%2Fjhep08%282016%29033.

[12] G. Hernández-Tomé et al. "Effects of heavy Majorana neutrinos on lepton flavor violating processes". In: *Physical Review D* 101.7 (Apr. 2020). DOI: 10.1103/physrevd.101.075020. URL: https://doi.org/10.1103%2Fphysrevd.101.075020.

[13] ATLAS collaboration. *ATLAS measures Higgs boson's decay width*. 2022. URL: https://home.cern/news/news/physics/atlas-measures-higgs-bosons-decay-width.

[14] J.A. Casas et al. "Reopening the Higgs portal for single scalar dark matter". In: *Journal of High Energy Physics* 2017.5 (May 2017). DOI: 10.1007/jhep05(2017)036. URL: https://doi.org/10.1007%2Fjhep05%282017%29036.

[15] James M. Cline et al. "Update on scalar singlet dark matter". In: *Physical Review D* 88.5 (Sept. 2013). DOI: 10.1103/physrevd.88.055025. URL: https://doi.org/10.1103%2Fphysrevd.88.055025.

[16] E. Aprile et al. “Dark Matter Search Results from a One Ton-Year Exposure of XENON1T”. In: *Physical Review Letters* 121.11 (Sept. 2018). DOI: 10.1103/physrevlett.121.111302. URL: https://doi.org/10.1103%2Fphysrevlett.121.111302.

[17] Gerard Jungman, Marc Kamionkowski, and Kim Griest. “Supersymmetric dark matter”. In: *Physics Reports* 267.5-6 (Mar. 1996), pp. 195–373. DOI: 10.1016/0370-1573(95)00058-5. URL: https://doi.org/10.1016%2F0370-1573%2895%2900058-5.

[18] Riccardo Catena and Bodo Schwabe. “Form factors for dark matter capture by the Sun in effective theories”. In: *Journal of Cosmology and Astroparticle Physics* 2015.04 (Apr. 2015), pp. 042–042. DOI: 10.1088/1475-7516/2015/04/042. URL: https://doi.org/10.1088%2F1475-7516%2F2015%2F04%2F042.

[19] Martin Asplund et al. “The Chemical Composition of the Sun”. In: *Annual Review of Astronomy and Astrophysics* 47.1 (Sept. 2009), pp. 481–522. DOI: 10.1146/annurev.astro.46.060407.145222. URL: https://doi.org/10.1146%2Fannurev.astro.46.060407.145222.

[20] N. Wyn Evans, Ciaran A. J. O’Hare, and Christopher McCabe. *SHM^{++}: A Refinement of the Standard Halo Model for Dark Matter Searches in Light of the Gaia Sausage*. 2018. arXiv: 1810.11468 [astro-ph.GA].

[21] Qinrui Liu et al. “χaroν: a tool for neutrino flux generation from WIMPs”. In: *Journal of Cosmology and Astroparticle Physics* 2020.10 (Oct. 2020), pp. 043–043. DOI: 10.1088/1475-7516/2020/10/043. URL: https://doi.org/10.1088%2F1475-7516%2F2020%2F10%2F043.

[22] Miguel Gutiérrez, Manuel Masip, and Sergio Muñoz. “The Solar Disk at High Energies”. In: *The Astrophysical Journal* 941.1 (Dec. 2022), p. 86. DOI: 10.3847/1538-4357/aca020. URL: https://doi.org/10.3847%2F1538-4357%2Faca020.

UNIVERSIDAD DE GRANADA

PROPUESTA DE TRABAJO FIN DE MÁSTER EN FÍSICA

Escuela Internacional de Posgrado

MASTER EN FÍSICA; CURSO 2022 – 2023

TUTOR/A: Manuel Masip Mellado
DEPARTAMENTO: Física Teórica y del Cosmos
CO-TUTOR/A:
DEPARTAMENTO:

TÍTULO DEL TRABAJO: Producción de neutrinos solares de alta energía en un modelo de materia oscura

INTRODUCCIÓN:
El universo contiene 5 gramos de materia oscura (MO) por cada gramo de materia visible. La naturaleza de la partícula que constituye dicha MO es todavía desconocida, pero se investiga activamente tanto en experimentos de búsqueda directa (sus colisiones elásticas con núcleos pesados) como indirecta (su aniquilación con una antipartícula de MO podría producir una señal de alta energía procedente del sol o el centro galáctico).

OBJETIVOS:
Nuestro objetivo es definir un modelo viable de MO cuya aniquilación produzca una señal óptima en telescopios de neutrinos. Se comprobará que dicho modelo es capaz de explicar la abundancia de materia oscura que observamos y se obtendrá el flujo de neutrinos de alta energía procedentes del sol predichos por el modelo en el observatorio KM3NeT.

METODOLOGÍA:
Estudio del modelo cosmológico de Big Bang. Definición del modelo de MO y elaboración de un código informático para el cálculo de su abundancia en la actualidad. Determinación del flujo de neutrinos procedentes del sol en KM3NeT, aspecto este último para el que se contará con la colaboración de Miguel Gutiérrez González (miembro de KM3NeT).

BIBLIOGRAFÍA:

[1] L. Bergstrom, A. Goobar, *Cosmology and particle astrophysics,* Springer, 2004
[2] E.W. Kolb, M.S. Turner, *The Early Universe*, CRC Press, 1990

Alumno/a propuesto/a: Pablo de la Torre Domínguez

Fdo (Tutor/a): MASIP MELLADO MANUEL - 35043277V Digitally signed by MASIP MELLADO MANUEL - 35043277V Date: 2022.11.15 14:26:08 +01'00'

Fdo (Cotutor/a):

Fdo (Alumno/a): DE LA TORRE DOMINGUEZ PABLO - 54370415W Firmado digitalmente por DE LA TORRE DOMINGUEZ PABLO - 54370415W Fecha: 2022.11.20 17:33:29 +01'00'

Granada, 15 de noviembre de 2022